THE JOURNAL OF PHYSICAL CHEMISTRY C

ARTICLE

pubs.acs.org/JPCC

New Insights into the Early Stages of Nanoparticle Electrodeposition

Jon Ustarroz,[†] Xiaoxing Ke,[‡] Annick Hubin,[†] Sara Bals,[‡] and Herman Terryn*[,†]

[†]Research Group Electrochemical and Surface Engineering (SURF), Vrije Universiteit Brussel, Pleinlaan 2, 1050 Brussels, Belgium

[‡]EMAT, University of Antwerp, Groenenborgerlaan 171, 2020 Antwerp, Belgium

Supporting Information

ABSTRACT: Electrodeposition is an increasingly important method to synthesize supported nanoparticles, yet the early stages of electrochemical nanoparticle formation are not perfectly understood. In this paper, the early stages of silver nanoparticle electrodeposition on carbon substrates have been studied by aberration-corrected TEM, using carbon-coated TEM grids as electrochemical electrodes. In this manner we have access to as-deposited nanoparticle size distribution and structural characterization at the atomic scale combined with electrochemical measurements, which represents a breakthrough in a full understanding of the nanoparticle electrodeposition mechanisms. Whereas classical models, based upon characterization at the nanoscale, assume that electrochemical growth is only driven by direct attachment, the results reported hereafter indicate that early nanoparticle growth is mostly driven by nanocluster surface movement and aggregation. Hence, we conclude that electrochemical nulceation and growth models should be revised and that an electrochemical aggregative growth mechanism should be considered in the early stages of nanoparticle electrodeposition.

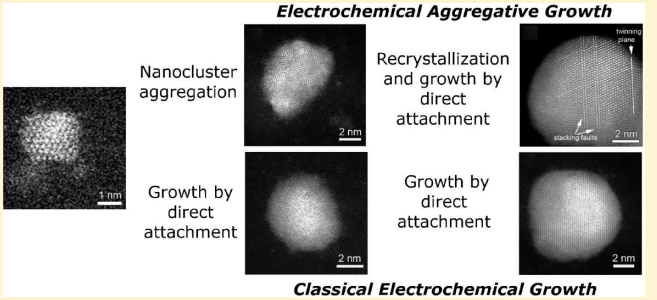

INTRODUCTION

Recently, electrochemical deposition is arising as a promising technique to synthesize supported nanoparticles which are important for many applications including electrocatalysis[1] and electroanalysis.[2] By means of electrochemical deposition, nanoparticles grow direclty from the substrate without the need of further sample preparation. Moreover, the technique is surfactant-free and cost-effective and allows to tune the nature of the nanoclusters by changing electrolyte composition and deposition parameters.[3] Several groups have electrodeposited metallic nanoparticles on various substrates such as glassy carbon,[4,5] highly oriented pyrolitic graphite,[6,7] indium-doped tin oxide,[8,9] carbon nanotubes,[10] and others.[11] However, in order to investigate the size-dependent properties of small nanoparticles and to use them as electrocatalysts or in sensing devices, distributions with low size dispersions need to be obtained. This still represents a challenge in the field of electrochemical deposition. In order to overcome this issue and improve nanoscale electrodeposition, it becomes extremely important to understand nanocluster nucleation and growth.

Since many decades plenty of theoretical and experimental literature is available reviewing this topic,[3,12−14] with the most widely referred model being the one developed by Scharifker and Hills,[15] which has been slightly reformulated several times.[16−18] Conventionally, electrochemical nucleation and growth studies have been addressed indirectly by measuring the current−time transients in potentiostatic experiments and correlating them to models that take into account the random nature of nucleation and the coupled growth of hemispherical nuclei under diffusion limitations. According to these models, an electrochemically formed nucleus grows by direct reduction of ions onto its surface if this action is thermodynamically favorable (i.e., if the Gibbs free energy is reduced by the addition of more atoms to the cluster), whereas it will dissolve if this condition is not fulfilled. Therefore, it has been normally considered that when a constant overpotential is applied, nuclei whose radii are bigger than a critical radius (r_c) are formed progressively in the surface and grow by direct attachment. The growth of each of them affects both the concentration of active species and the overpotential distribution in the cluster vicinity creating zones of reduced concentration and overpotential and thus reduced nucleation rate. Then, if multiple clusters are considered, their local zones of reduced nucleation rate spread and gradually overlap. This is a very complex problem which is frequently solved by approximating the areas of reduced nucleation rate by overlapping planar diffusion zones in which nucleation is fully arrested.[15−18] It is then foreseen that for progressive nucleation the number of growing nuclei can be expressed by an exponential law:

$$N(t) = N_0[1 - \exp(-At)] \quad (1)$$

where N_0 is the total number of active sites and A is the nucleation rate constant. Under these conditions, average particle size

Received: October 26, 2011
Revised: December 19, 2011
Published: December 23, 2011

and size dispersion should increase with time. This formula accounts for progressive nucleation, but instantaneous nucleation can be thought as the limit in which $A \rightarrow \infty$ and then $N = N_0$, so N_0 nuclei are instantaneously formed at $t = 0$.

Then, if it is considered that these growth centers which are randomly distributed on the electrode surface grow under spherical diffusion control, the total electrochemical current can be expressed by

$$I(t) = \beta zFc\left(\frac{D}{\pi t}\right)^{1/2}\left[1 - \exp\left(-\frac{1}{2}AN_0\pi\gamma\left(\frac{8\pi cM}{\rho}\right)^{1/2}Dt^2\right)\right] \quad (2)$$

if the nucleation is progressive and

$$I(t) = zFc\left(\frac{D}{\pi t}\right)^{1/2}\left[1 - \exp\left(-N_0\pi\left(\frac{8\pi cM}{\rho}\right)^{1/2}Dt\right)\right] \quad (3)$$

if the nucleation is instantaneous. F is the Faraday constant, z is the valence of the metal ions, c is the electrolyte concentration, D is the diffusion coefficient, β equals 1 according to refs 15 and 16 and equals 4/3 according to refs 17 and 18, and γ equals 4/3 according to refs 13, 15, and 19 and equals 1 according to the other references. We will consider $\beta = 1$ and $\gamma = 4/3$.

Nevertheless, all these models have been based on nanometer scale characterization because the attachment of the nanoparticles to a surface, inherent to any electrodeposition process, has restricted the range of applicable techniques to surface techniques such as field emission scanning electron microscopy (FESEM)[4,5,11] or atomic force microscopy/scanning tunneling microscopy (AFM/STM).[6,20−22] However, it becomes clear that when the early stages of nucleation and growth need to be explained, accurate characterization at the atomic scale is indispensible. Therefore, controversy still remains about their validity.[12,23] In fact, a very interesting approach to combine TEM resolution with in situ time-resolved measurements showed that classical models do not explain growth kinetics in detail.[23−26] Unfortunately, the fact that the electrons had to be transmitted through the electrolyte made their TEM spatial resolution rise up to about 5 nm, making impossible to detect smaller nuclei and to reach atomic scale characterization.

Recently, an innovative and straightforward approach to access atomic resolution characterization on as-electrodeposited nanoparticles was achieved by using carbon-coated gold TEM grids as substrates for the electrodeposition of silver nanoparticles.[27] In this manner, the actual particle size distribution and atomic scale structural information can be correlated with electrochemical measurements yielding unique information required for a full understanding of the early stages of electrochemical nanoparticle formation.

In this paper, we study the early stages of electrochemical nucleation and growth of silver nanoparticles on carbon substrates by aberration-corrected TEM. By the use of carbon-coated TEM grids as electrochemical electrodes, we get direct access to electrochemically deposited nanoparticle size distribution and structural characterization at the atomic scale, directly combined with electrochemical measurements. We show that even if electrochemical measurements fit with existing electrochemical nucleation and growth models, these models fail to describe the nanoscale phenomena observed during the early stages of nanoparticle electrodeposition on low-energy substrates such as carbon. Finally, we describe a revision of the classical electrochemical models, indicating that surface movement of nanoclusters and aggregation must be considered during the early stages of electrochemical new phase formation.

EXPERIMENTAL METHODS

Experiments were carried out using a fresh solution of 0.1 M KNO_3 + 1 × 10^{-3} M $AgNO_3$ previously deareated with high-purity N_2. Electrochemical measurements were performed with an Autolab PGSTAT12 potentiostat in a standard three-electrode cell with Ag/AgCl reference electrode and Pt counter electrode. The working electrodes were carbon-coated gold TEM grids from EMS (300 mesh, CF 300Au). More details about the use of carbon-coated TEM grids as electrodes can be found in the Supporting Information (Figure S1). Morphological and structural characterization of the electrodeposited nanoparticles was performed using a FEI Tecnai G2 TEM operated at 200 kV and using a FEI Titan 50-80 TEM operated at 300 kV. Size and spatial distribution and atomic scale structural configuration were investigated by aberration-corrected high angle annular dark field scanning transmission electron microscopy (HAADF-STEM) and high resolution transmission electron microscopy (HRTEM). The probe corrected HAADF-STEM images were acquired using a semiconvergence angle of 24.1 mrad.

RESULTS AND DISCUSSION

Electrochemical Measurements on Carbon-Coated TEM Grids. Potentiostatic single pulse depositions were performed by pulsing the electrode potential to −400 mV vs Ag/AgCl, where the process should be diffusion controlled and no other reactions such as hydrogen evolution are present. The nucleation and growth phenomena of the early stages of silver nanoparticle electrodeposition onto the TEM grids can then be analyzed according to the classical electrochemical models by means of their chronoamperommetric response as shown in Figure 1a. The initial high current at $t = 0$ and fast current decay (0−1 ms) have been many times attributed to the double-layer charging.[15,28] The following increase of current is characteristic of nucleation and growth processes because of the increasing number of nuclei of the new phase in the electrode surface. The current peak and posterior decrease is caused by the coalescence of the diffusion zones of the growing particles.[5,15,20] The characteristic peaked shape of these current transients suggests that they can be analyzed according to the theoretical models proposed by Scharifker and Hills[15] which include progressive (or instantaneous) nucleation and diffusion-controlled growth of hemispherical particles taking in account the overlapping of their diffusion zones. Thus, the current transients for progressive and instantaneous nucleation can be described in a nondimensional form.[15]

It is shown in Figure 1b that the nondimensional form of the current−time transients obtained from the nucleation of silver on the carbon-coated TEM grids fits with the model for progressive nucleation if the induction period is not taken in account. The fact that the potentiostatic current transients satisfy the Scharifker−Hills model for progressive nucleation implies that the dimensional chronoamperogram can be fitted to eq 2 so that the nucleation rate AN_0 is obtained. The two unknowns AN_0 and D are obtained by fitting the experimental chronoamperogram to the model. A nonlinear fitting procedure is carried out

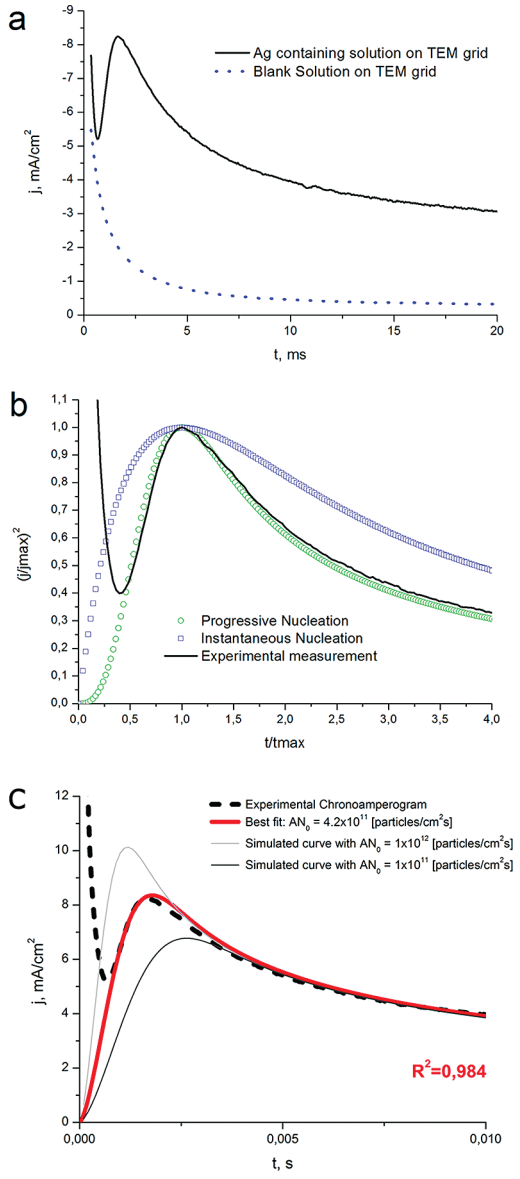

Figure 1. (a) Current transient for electrocrystallization of silver at −400 mV vs Ag/AgCl onto a carbon-coated TEM grid. The dotted line represents the current transient recorded at same conditions in a silver free blank solution. (b) Nondimensional plot of the current transient for electrocrystallization of silver at −400 mV vs Ag/AgCl compared to the Scharifker−Hills theoretical models for instantaneous and progressive nucleation. (c) Experimental chronoamperogram of the potentiostatic electrodeposition of silver at −400 mV vs Ag/AgCl and dimensional plots of the Scharifker−Hills model for progressive nucleation (eq 2) with different values of the nucleation rate constant AN_0.

using the Levenberg−Marquardt algorithm available in OriginPro. Very good agreement is obtained with the best fitting parameters being $AN_0 = 4.21 \times 10^{11} \pm 5.69 \times 10^9$ particles/cm^2 and $D = 5.16 \times 10^{-5} \pm 2.21 \times 10^{-7}$ cm^2/s. The adjusted R^2 coefficient is found to be 0.984, indicating a very good correlation between the experimental data and the model. Figure 1c shows the experimental chronoamperogram and the theoretical model for the best fitting parameters and different values of AN_0.

As mentioned previously, those equations assume that the number of nuclei grows with time according to eq 1. This means that if it is possible to determine experimentally $N(t)$, it is possible to fit these data to an exponential curve to obtain A and N_0. Such measurements and calculations are typical from electrochemical nucleation and growth studies, sometimes with good agreement[21] and sometimes without.[23,26] Unfortunately, disagreement among different studies is probably due to the fact that the resolution of the equipments used to characterize the electrodeposited nuclei plays an important role in the determination of $N(t)$.

TEM Characterization of As-Electrodeposited Nanoparticles. HAADF-STEM images are used to determine the nanoparticle size distribution after applying potentiostatic single pulses for different deposition times, in which the potential was kept on −400 mV vs Ag/AgCl. Typical HAADF-STEM pictures of low (a) and high (b) magnification are shown in Figure 2. Two populations are clearly distinguished corresponding to a bimodal size distribution in which "large" particles have $d \geq 6$ nm, whereas the diameter of the "small" particles is always smaller than 2.5 nm.[27] "Low" magnification pictures are used to determine the size distribution of "large" particles, whereas the size distribution of "small" particles is deduced from the "high" magnification pictures.

Figure 2 shows the evolution of diameter (d) and particle density (e) as a function of deposition time. The number of "large" particles grows exponentially with time until it becomes saturated after 30 ms with a value around 6×10^7 particles/cm^2. Accordingly, their average diameter and size dispersion also grow with time from $d = 10 \pm 4$ nm for $t = 1$ ms to $d = 45 \pm 29$ nm for $t = 500$ ms. On the other hand, the number of randomly dispersed "small" particles also grows with time during the first 10 ms but then decreases during the following 20−30 ms. For longer times, the number of those kinds of particles is negligible. Surprisingly, the size of these particles remains constant with $d = 1.70 \pm 0.55$ nm, independently of the deposition time. Actually, if we look at the evolution of the number of "large" nanoparticles with time $N(t)$, we clearly identify an exponential behavior which agrees with eq 1, being $A = 92 \pm 43$ s^{-1} and $N_0 = 5.28 \times 10^9 \pm 8.85 \times 10^8$ particles/cm^2 the best fitting parameters (see Figure 2f). The product of these two values gives $AN_0 = 4.86 \times 10^{11}$ particles/(cm^2 s), which is almost equal to the value obtained from the fitting of the chronoamperommetric curve to eq 2. This means that the evolution with time of the "large" particle distribution agrees with the classical progressive nucleation model. However, the presence of a bimodal size distribution in the early stages of the process in which such "large" growing particles coexist with randomly dispersed "small" clusters cannot be predicted by the classical models. In fact, it is logical that the nucleation of the "small" clusters is not reflexed by the chronoamperograms because their contribution to the total current compared to the larger particles is very small. Though, the understanding of why these nuclei are present and which parameters may affect their size and number density is certainly of great importance for nanoscale electrodeposition, especially when the obtention of small nanoparticles ($d \leq$ 10−15 nm) is aimed.

In addition, it is shown in Figure 2c that not all the "small" clusters are randomly distributed all throughout the surface, but a significant concentration of them is frequently observed surrounding the "large" particles in a satellite-like disposition. According to the classical island growth mechanism, nuclei should be randomly distributed all throughout the substrate unless in defect-rich regions, where the thermodynamic work for nucleation is lower. The observed satellite-like disposition (Figure 2c) is not likely to be originated by defects unless the

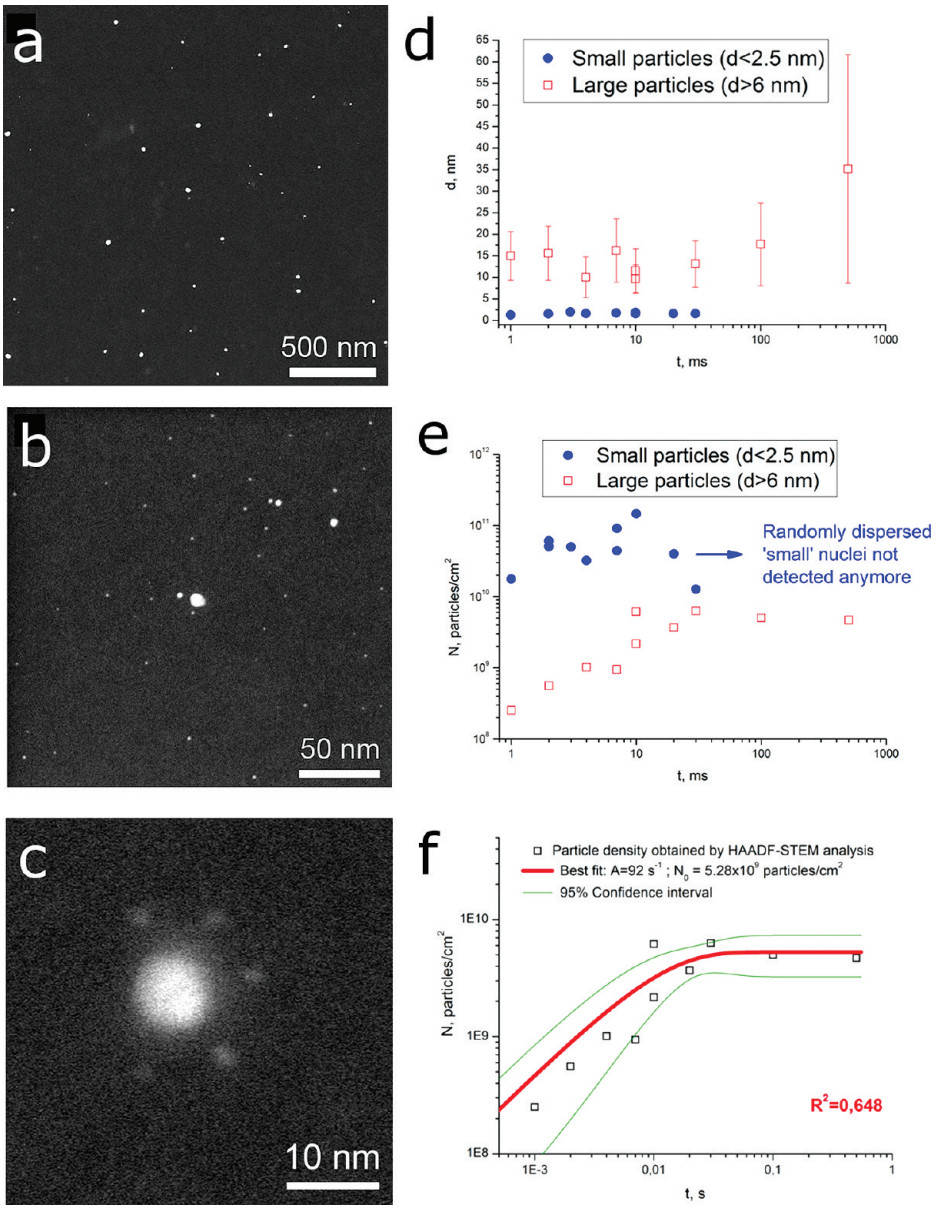

Figure 2. Typical low (a) and high (b) magnification HAADF-STEM pictures after potentiostatic electrodeposition of silver at −400 mV vs Ag/AgCl during 7 ms. (c) Typical HAADF-STEM picture showing a bigger concentration of "small" nuclei surrounding a "large" particle in a satellite-like disposition. Evolution of "large" and "small" nanoparticle size (d) and number density (e) with deposition time obtained from the analysis of STEM pictures. (f) Evolution of "large" nanoparticle number density with deposition time obtained from the analysis of HAADF-STEM pictures and the best exponential fit of eq 1.

presence of a growing "large" particle distorted the substrate in such a way that defects were originating around it. However, these satellite-like rings would fall within the limits of the nucleation exclusion zone of the growing particle so the likelihood that new nuclei were being originated there would be minimum, definitely not enough to explain such a high nuclei density. Neither this observation can be predicted by electrochemical nucleation and growth models which are based on random nucleation.

On the other hand, it is relevant to study possible compositional or structural differences among "large" and "small" particles which might explain their different growth kinetics. It is known that in some cases silver may be oxidized when electrodeposited from an aqueous solution; therefore, it is important to determine whether the particles are pure silver or a silver oxide phase is also present. Here, HTREM and probe corrected HAADF-STEM images along with their fast Fourier transform (FFT) patterns confirm that all the electrodeposited nanoparticles are pure silver independently from their size (see Supporting Information Figure S4).

In addition, probe corrected HAADF-STEM is used to investigate whether the particles are monocrystalline, polycrystalline, or aggregates. Figure 3 shows characteristic HAADF-STEM images of the different sizes of silver nanoparticles electrochemically grown on the carbon film. Far more than half of the larger particles ($d \geq 15$ nm) are monocrystalline with defects such as stacking faults and twinnings (Figure 3a,b), whereas about the same fraction of medium sized particles

dx.doi.org/10.1021/jp210276z |J. Phys. Chem. C 2012, 116, 2322–2329

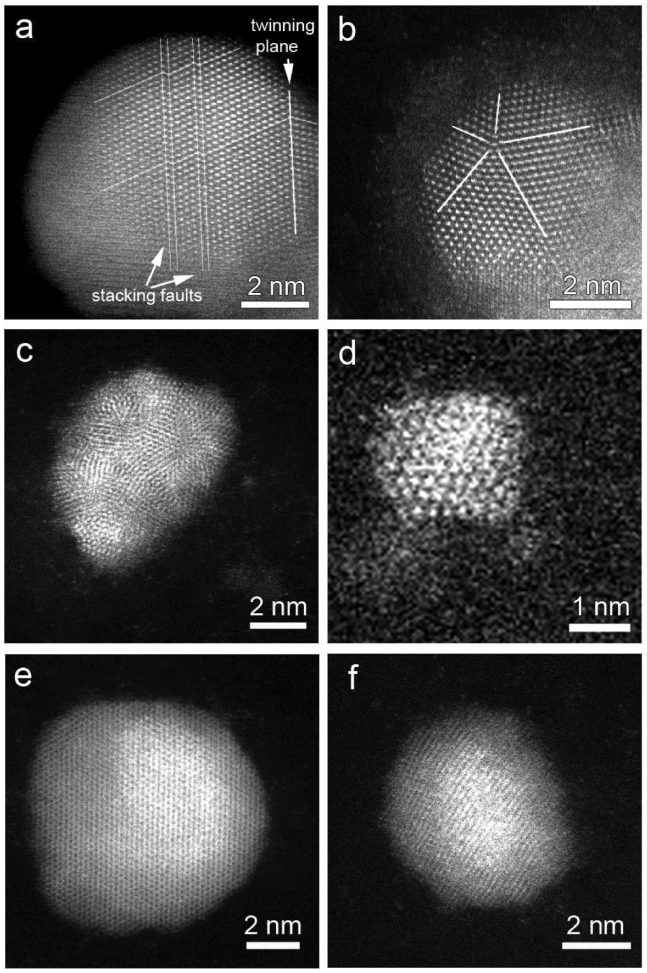

Figure 3. (a) "Large" monocrystalline particle with defects of stacking faults and twinning planes as indicated. (b) "Large" monocrystalline particle with 5-fold twinning planes as indicated. (c) "Medium-sized" polycrystalline nanoparticle. (d) Ultrasmall nanoparticle with low crystallinity. (e) "Large" monocrystalline particle without defects. (f) "Medium sized" monocrystalline nanoparticle.

($6 \leq d \leq 15$ nm) presents polycrystalline structures in which the crystalline domains have dimensions ranging from 1 to 3 nm (Figure 3c). Besides, a small fraction of the larger particles has also been found to be monocrystalline without defects (Figure 3e), whereas about the same small fraction of medium sized nanoparticles (Figure 3f) has been found to be monocrystalline. In addition, the arrangement of the atoms in the "small" clusters becomes less ordered so the degree of crystallinity decreases as shown in Figure 3d.

According to the classical models, the main mechanism in which a particle grows is by direct reduction of ions from the electrolyte on the island surface. However, if this would be the case, most of the as-electrodeposited nanoparticles should present a monocrystalline structure. Therefore, the fact that in the early growth stages most of the "medium sized" nanoparticles are polycrystalline with crystalline domains with similar size to the "small" clusters (Figure 3c,d) suggests that another mechanism such as aggregation−coalescence of small clusters governs the early electrochemical growth of the nanoparticles. The fact that larger particles tend to be monocrystalline with defects (Figure 3a,b) can be explained by the tendency of polycrystalline nanoparticles to reduce its internal energy by recrystallizing into a monocrystalline structure[29] and indicates that further nanoparticle growth is again governed by direct attachment because otherwise larger nanoparticles should present polycrystalline domains at least in their outer surface.

Electrochemical Aggregative Growth Mechanism. In conclusion, the data presented throughout this paper indicate that classical electrochemical nucleation and growth theories do not fully account for some nanoscale phenomena occurring during the early stages of silver electrodeposition. Hence, we suggest that an electrochemical aggregative growth mechanism might be the clue to understanding the observed phenomena on the early stages of electrochemical nanoparticle formation and growth. Figure 4 represents schematically the stages of the proposed mechanism.

In the first instants after the application of a negative potential, very small clusters of $r \approx r_c$ are formed randomly distributed through the carbon substrate (particles such as 1 in Figure 4a). Even at these early stages, some clusters have been formed so close to each other that they have already coalesced in "medium sized" particles which are henceforward called first-order agglomerates (particles such as 3 in Figure 4b). Then, as the nucleation is progressive, more small clusters will be formed until the nucleation exclusion zones have overlapped and covered all the surface. Although those small clusters do not dissolve because $r \geq r_c$, they have high energy (large surface to volume ratio) and low degree of crystallinity (Figure 3d) so they are unstable, and they can easily move through the surface because of their small size[30] and the weak van der Waals forces between carbon and silver atoms.

We suggest that some of the small clusters aggregate with each other forming more first-order agglomerates and that some others are attracted toward the larger agglomerates, ending up coalescing with them. The reason why we propose this mechanism is that most of the "medium sized" particles are polycrystalline with crystalline domains of the size of the small clusters as shown in Figure 3e. In addition, the satellite-like disposition of particles which is found surrounding the larger clusters (Figure 2c and particles such as 2 in Figure 4b) would support this theory. This aggregation mechanism takes place due to a thermodynamic driving force altering the system toward its lowest energy configuration as small nuclei may move through the surface because of the same reasons than adatoms move toward edges or kink sites.[30]

Then, until the conditions of planar diffusion are reached (i.e., when nucleation exclusion zones have overlapped and covered all the surface as in Figure 4c), three phenomena happen in parallel: nucleation of new small clusters; surface movement of small clusters which may aggregate with each other forming a new first-order aggregate or may be incorporated in an existing aggregate; direct attachment (i.e., incorporation of Ag^+ ions onto aggregates and small clusters). Even if far more than half of the nanoparticles at this stage are polycrystalline (Figure 3c and particles such as 3 in Figure 4b), a small fraction of monocrystalline structures (Figure 3f and particles such as 4 in Figure 4b) and aggregates (particles such as 6 in Figure 4c) has also been found. Therefore, we suggest that both aggregation and direct attachment are responsible for such early nanoparticle growth, being aggregation predominant over the classical growth mechanism. Afterward, when nucleation exclusion zones have completely covered the surface (Figure 4c), no more nucleation is supposed to happen in the carbon surface so the concentration of the randomly dispersed small clusters decreases due to their aggregation or incorporation in the first-order aggregates.

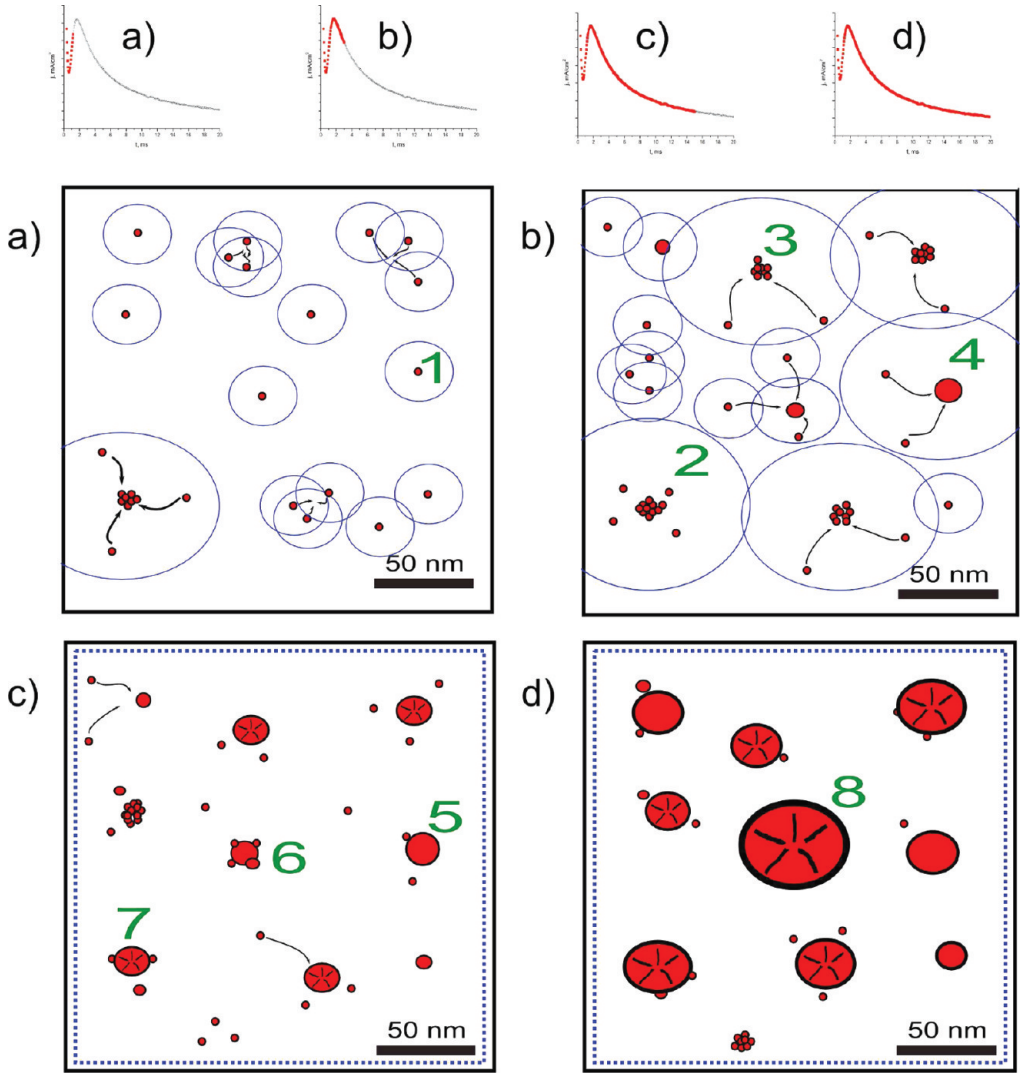

Figure 4. Electrochemical aggregative growth mechanism. Red dots represent the nanoparticles, and blue circles are the projection of their corresponding nucleation exclusion zones. Black stripes within a particle represent defects, whereas the absence of stripes represents a defect-free monocrystalline structure.

Finally, when all the small clusters have been consumed (Figure 4d), the number of first-order aggregates reaches saturation. At this stage, previous polycrystalline and aggregated particles undergo recrystallization into monocrystalline structures so most of the larger particles are monocrystalline with a high amount of defects (Figure 3a,b and particles such as 7 and 8 in Figure 4c,d). In a few cases, monocrystalline "large" particles without defects are also found due to the growth of "medium sized" monocrystalline particles (Figure 3e and particles such as 5 in Figure 4c). In later stages, as no more small clusters are present in the carbon surface and nucleation exclusion zones cover all the carbon surface, further nanoparticle growth should be due to direct attachment. However, as long as large particles keep growing toward the macroscale, coalescence among them is also expected, forming second- and higher-order aggregates until all the carbon surface is covered by silver.

The most significant feature introduced by the proposed mechanism is that in the early stages of electrochemical nucleation and growth surface movement and aggregation of clusters of $d \approx 1-2$ nm cannot be considered negligible and determine to a great extent the size and structure of electrodeposited nanostructures. This is a striking result not only because these mechanisms have never been considered in the widely accepted electrochemical models for nucleation and growth but also because as a result, nanoparticles on the early stages of their electrochemical growth are polycrystalline instead of monocrystalline, which is the most commonly accepted hypothesis. Obviously, this is of great importance in view of applications because the crystalline structure of the nanoparticles will radically influence their electrocatalytic and other properties.

Even if to the best of our knowledge such growth model has not been reported in the field of electrochemical new phase formation, some groups have already discussed similar results in the field of colloidal synthesis of nanocrystals.[29,31−34] According to these studies, the presence of bimodal size distributions in the early stages of nucleation as well as the polycrystallinity of the nanoparticles can be explained by an aggregative growth mechanism. One important difference between colloidal synthesis and electrodeposition is that in the latter case the nucleation, growth, and movement of nuclei are limited to the electrode surface.

dx.doi.org/10.1021/jp210276z |J. Phys. Chem. C 2012, 116, 2322–2329

Even if an aggregative growth mechanism has never been discussed in the field of electrodeposition, a similar mechanism called Smoluchowski ripening, which involves surface diffusion and coalescence of clusters, has also been attributed to the coarsening of nanoparticles supported on metallic surfaces due to thermal activation.[30,35−37] Bimodal size distributions in electrochemical systems have been sometimes associated with electrochemically induced Ostwald ripening,[38,39] but HR-(S)TEM was never performed so the crystallinity of the particles was not checked. An Ostwald ripening process implies single atom dissolution/deposition so it should not give rise to polycrystalline nanoparticles. Therefore, we believe that such electrochemically facilitated surface diffusion process might have been aggregative−coalescence processes rather than Ostwald ripening.

The proposed mechanism, although being substantially different from the classical approach, allows a similar interpretation of the potentiostatic current transients in terms of nucleation and growth models. As it has been demonstrated in previous sections, the SH model of progressive nucleation is in good agreement with the number of "large" particles (or first-order aggregates) determined by HAADF-STEM imaging. In fact, the current measured due to silver reduction is exactly the same whether silver atoms incorporate directly onto a growing particle or a cluster is first formed on the substrate and is incorporated in an aggregate after moving through the surface. On the other hand, in classical nucleation and growth models, $N(t)$ is just assumed as the number of particles which are contributing to the current by becoming larger each time, and it is described as an exponential law because of the random nature of nucleus formation accounting for the nucleation exclusion zones[12] Therefore, $N(t)$ can describe in the same way the progressive nature of the creation of first-order aggregates. This means that no matter how the particles or aggregates grow, their contribution to the measured current, and thus the relation between chronoamperograms and $N(t)$ through the nucleation and growth models, will be the same whenever $N(t)$ is considered as the number of growing particles of aggregates.

CONCLUSIONS

In conclusion, we have discovered new insights into the early stages of nanoparticle electrodeposition on low-energy substrates such as carbon by the use of carbon-coated TEM grids as electrochemical working electrodes. Whereas classical models assume that electrochemical growth is only driven by direct attachment, we have found proof that nanocluster surface movement and aggregation cannot be neglected. A bimodal size distribution is found since the very early stages of nucleation. Whereas "larger" clusters grow in number and size with time according to conventional electrochemical nucleation and growth models, "small" clusters of $d \approx 1-2$ nm do not to grow and diminish in number after a certain deposition time. A bigger concentration of those "small" nuclei is frequently found to be surrounding the "large" particles in a satellite-like disposition. Structural characterization by means of HR-(S)TEM reveals that "medium size" nanoparticles are in most of the cases polycrystalline, suggesting that direct attachment cannot be the only early growth mechanism. The reported results indicate that classical electrochemical nucleation and growth theories do not fully account for the nanoscale phenomena happening during the early stages of nanoparticle electrodeposition. Hence, we have proposed an electrochemical aggregative growth mechanism which takes in account surface nanocluster movement and coalescence. In view of the importance of electrodeposition as a method to syntesize nanostructured materials which have applications in several areas such as electrocatalysis or electroanalysis, the understanding of the mechanisms underlying nanoparticle growth in an electrodeposition process becomes extremely important because it influences nanoparticle size distribution and crystal structure, which determine the properties of any nanostructured material.

ASSOCIATED CONTENT

Supporting Information. Use of carbon-coated TEM grids as electrochemical electrodes; HRTEM and probe corrected HAADF-STEM fast Fourier transform (FFT) patterns. This material is available free of charge via the Internet at http://pubs.acs.org.

AUTHOR INFORMATION

Corresponding Author
*E-mail: hterryn@vub.ac.be.

ACKNOWLEDGMENT

The authors acknowledge the support from the Fonds Wetenschappelijk Onderzoek in Vlaanderen (FWO, Contract FWOAL527), the Flemish Hercules 3 programme for large infrastructure, and the Société Française de Bienfaisance et d'Enseignement (S.F.B.E.) de San Sebastian-Donostia (Spain).

REFERENCES

(1) Campelo, J. M.; Luna, D.; Luque, R.; Marinas, J. M.; Romero, A. A. *ChemSusChem* **2009**, *2*, 18–45.
(2) Welch, C. W.; Compton, R. G. *Anal. Bioanal. Chem.* **2006**, *384*, 601–619.
(3) Staikov, G. *Electrocrystallization in Nanotechnology*; Staikov, G., Ed.; Wiley-VCH Verlag GmbH & Co. KGaA: Weinheim, 2007.
(4) Isse, A. A.; Gottardello, S.; Maccato, C.; Gennaro, A. *Electrochem. Commun.* **2006**, *8*, 1707–1712.
(5) Komsiyska, L.; Staikov, G. *Electrochim. Acta* **2008**, *54*, 168–172.
(6) Zoval, J. V.; Lee, J.; Gorer, S.; Penner, R. M. *J. Phys. Chem. B* **1998**, *102*, 1166–1175.
(7) Liu, H.; Favier, F.; Ng, K.; Zach, M. P.; Penner, R. M. *Electrochim. Acta* **2001**, *47*, 671–677.
(8) Ueda, M.; Dietz, H.; Anders, A.; Kneppe, H.; Meixner, A.; Plieth, W. *Electrochim. Acta* **2002**, *48*, 377–386.
(9) Ma, Y. T.; Di, J. W.; Yan, X.; Zhao, M. L.; Lu, Z. J.; Tu, Y. F. *Biosens. Bioelectron.* **2009**, *24*, 1480–1483.
(10) Day, T. M.; Unwin, P. R.; Macpherson, J. V. *Nano Lett.* **2007**, *7*, 51–57.
(11) Sheridan, E.; Hjelm, J.; Forster, R. J. *J. Electroanal. Chem.* **2007**, *608*, 1–7.
(12) Hyde, M. E.; Compton, R. G. *J. Electroanal. Chem.* **2003**, *549*, 1–12.
(13) Plieth, W. In *Electrochemistry for Materials Science*; Plieth, W., Ed.; Elsevier B.V.: Amsterdam, 2008.
(14) Paunovic, M. *Fundamentals of Electrochemical Deposition*; Wiley-Interscience: New York, 2006.
(15) Scharifker, B.; Hills, G. *Electrochim. Acta* **1983**, *28*, 879–889.
(16) Scharifker, B. R.; Mostany, J. *J. Electroanal. Chem.* **1984**, *177*, 13–23.
(17) Mirkin, M. V.; Nilov, A. P. *J. Electroanal. Chem.* **1990**, *283*, 35–51.
(18) Heerman, L.; Tarallo, A. *Electrochem. Commun.* **2000**, *2*, 85–89.

(19) Correia, A. N.; Machado, S. A. S.; Avaca, L. A. *J. Electroanal. Chem.* **2000**, *488*, 110–116.
(20) Grujicic, D.; Pesic, B. *Electrochim. Acta* **2002**, *47*, 2901–2912.
(21) Hyde, M. E.; Jacobs, R.; Compton, R. G. *J. Phys. Chem. B* **2002**, *106*, 11075–11080.
(22) Simm, A. O.; Ji, X. B.; Banks, C. E.; Hyde, M. E.; Compton, R. G. *ChemPhysChem* **2006**, *7*, 704–709.
(23) Radisic, A.; Vereecken, P. M.; Hannon, J. B.; Searson, P. C.; Ross, F. M. *Nano Lett.* **2006**, *6*, 238–242.
(24) Williamson, M. J.; Tromp, R. M.; Vereecken, P. M.; Hull, R.; Ross, F. M. *Nature Mater.* **2003**, *2*, 532–536.
(25) Radisic, A.; Ross, F. M.; Searson, P. C. *J. Phys. Chem. B* **2006**, *110*, 7862–7868.
(26) Radisic, A.; Vereecken, P. M.; Searson, P. C.; Ross, F. M. *Surf. Sci.* **2006**, *600*, 1817–1826.
(27) Ustarroz, J.; Gupta, U.; Hubin, A.; Bals, S.; Terryn, H. *Electrochem. Commun.* **2010**, *12*, 1706–1709.
(28) Palomar-Pardavé, M.; Miranda-Hernández, M.; González, I.; Batina, N. *Surf. Sci.* **1998**, *399*, 80–95.
(29) Zheng, H. M.; Smith, R. K.; Jun, Y. W.; Kisielowski, C.; Dahmen, U.; Alivisatos, A. P. *Science* **2009**, *324*, 1309–1312.
(30) Zhang, Z. Y.; Lagally, M. G. *Science* **1997**, *276*, 377–383.
(31) Njoki, P. N.; Luo, J.; Kamundi, M. M.; Lim, S.; Zhong, C. J. *Langmuir* **2010**, *26*, 13622–13629.
(32) Richards, V. N.; Rath, N. P.; Buhro, W. E. *Chem. Mater.* **2010**, *22*, 3556–3567.
(33) Shields, S. P.; Richards, V. N.; Buhro, W. E. *Chem. Mater.* **2010**, *22*, 3212–3225.
(34) Richards, V. N.; Shields, S. P.; Buhro, W. E. *Chem. Mater.* **2011**, *23*, 137–144.
(35) Wen, J. M.; Evans, J. W.; Bartelt, M. C.; Burnett, J. W.; Thiel, P. A. *Phys. Rev. Lett.* **1996**, *76*, 652–655.
(36) Van Hyning, D. L.; Klemperer, W. G.; Zukoski, C. F. *Langmuir* **2001**, *17*, 3128–3135.
(37) Thiel, P. A.; Shen, M.; Liu, D. J.; Evans, J. W. *J. Phys. Chem. C* **2009**, *113*, 5047–5067.
(38) Redmond, P. L.; Hallock, A. J.; Brus, L. E. *Nano Lett.* **2005**, *5*, 131–135.
(39) Dudin, P. V.; Unwin, P. R.; Macpherson, J. V. *J. Phys. Chem. C* **2010**, *114*, 13241–13248.